

Some Climatological Aspects of the Madden–Julian Oscillation (MJO)

DONALD M. LAFLEUR, BRADFORD S. BARRETT, AND GINA R. HENDERSON

Oceanography Department, U.S. Naval Academy, Annapolis, Maryland

(Manuscript received 17 October 2014, in final form 4 March 2015)

ABSTRACT

One of the most commonly used metrics for both locating the Madden–Julian oscillation (MJO) geographically and defining the intensity of MJO convective activity is the real-time multivariate MJO (RMM) index. However, a climatology of the MJO, particularly with respect to the frequency of activity levels or of consecutive days at certain activity thresholds, does not yet exist. Thus, several climatological aspects of the MJO were developed in this study: 1) annual and 2) seasonal variability in MJO intensity, quantified using four defined activity categories (inactive, active, very active, and extremely active); 3) persistence in the above-defined four categories; 4) cycle length; and 5) low-frequency (decadal) variability.

On an annual basis, MJO phases 1 and 2 occurred more often, and phase 8 occurred less often, than the other phases throughout the year. Notable seasonality was also found, particularly in the frequency of extremely active MJO in March–May (8% of days) compared with June–August (only 1% of days). The MJO was persistent in time and across intensity categories, and all activity categories the following day had at least an 80% chance of maintaining their amplitudes. Implications of this climatology are discussed, including length of complete MJO cycles (the shortest of which was 17 days) and correlations between MJO amplitude and atmospheric response.

1. Introduction

Intraseasonal oscillations, such as the Madden–Julian oscillation (MJO; [Madden and Julian 1971](#)), are significant drivers of tropical and extratropical atmospheric circulation on time periods from 15 to 90 days ([Madden and Julian 1972](#); see also reviews by [Madden and Julian 1994](#); [Zhang 2005, 2013](#), and references therein). Of these, the MJO is the leading mode of intraseasonal variability in the tropics, with a period of roughly 30–60 days ([Madden and Julian 1972](#); [Knutson and Weickmann 1987](#); [Salby and Hendon 1994](#); [Wheeler and Kiladis 1999](#); [Majda and Stechmann 2012](#)). In the Indian and western Pacific Oceans, the MJO is primarily characterized by a broad region of anomalous circulation and convection that collectively propagates eastward at approximately 5 m s^{-1} . From the eastern Pacific Ocean across to Africa, the MJO is often characterized by only anomalous circulation, and here it propagates eastward at a faster speed, around 15 m s^{-1} ([Madden](#)

and [Julian 1972](#); [Knutson and Weickmann 1987](#); [Hendon and Salby 1994](#); [Milliff and Madden 1996](#)). Seasonal variance in MJO amplitude has also been noted: seasonal maxima (minima) have been found in boreal winter (summer) ([Madden 1986](#); [Knutson and Weickmann 1987](#); [Matthews et al. 1996](#); [Masunaga 2007](#); [Zhang and Dong 2004](#)) and the strongest (weakest) variance has been found in March (August) ([Lawrence and Webster 2002](#); [Roundy and Frank 2004](#)).

As a result of more than four decades of research, the tropical convection associated with the MJO is known to exert significant regional and global influences in both the tropics and extratropics, both directly and indirectly ([Hoskins and Karoly 1981](#); [Sardeshmukh and Hoskins 1988](#); [Matthews et al. 2004](#)). One of the most commonly used metrics for both locating the MJO geographically and defining the intensity of MJO convective activity is the real-time multivariate MJO (RMM) index of [Wheeler and Hendon \(2004, hereafter WH04\)](#). However, a climatology of the MJO with respect to the frequency of activity levels or of consecutive days at certain activity thresholds does not yet exist, despite its global importance. As one such example, it is well known that the atmosphere responds to tropical forcing and that the greater the forcing, the greater the response (e.g.,

Corresponding author address: Bradford S. Barrett, Oceanography Department, U.S. Naval Academy, 572C Holloway Rd., Annapolis, MD 21402.
E-mail: bbarrett@usna.edu

Hoskins and Karoly 1981). However, what amplitude marks an “extreme” MJO event? Additionally, what duration would mark an extreme event? These questions remain largely unanswered. Therefore, in this study, we seek to fill this gap by developing a climatology of MJO activity, intensity, and duration, and we do so utilizing the RMM index. We recognize that there are many possible characteristics of the MJO on which we could focus our climatology, but motivated by the desire to provide an historical context to the intensity and duration of MJO events (and particularly so for very active and extreme MJO events), we focus our climatology primarily on aspects of MJO intensity and duration.

Indices used to quantify the MJO signal typically fall into one of three categories: cloudiness, dynamical, or combined cloudiness and dynamical (Straub 2013). Precipitation and OLR data are generally used in cloudiness-based indices (e.g., Rui and Wang 1990; Kiladis and Weickmann 1992; Hendon and Salby 1994; Hendon et al. 1999; Matthews and Kiladis 1999; Matthews 2000; Wheeler et al. 2000; Kemball-Cook and Weare 2001; Kessler 2001, Myers and Waliser 2003; Kiladis et al. 2005; Benedict and Randall 2007; Matthews 2008; Kiladis et al. 2009). Dynamical-based indices utilize signals from upper-tropospheric zonal winds (e.g., Knutson and Weickmann 1987; Pohl and Matthews 2007; Chen and Del Genio 2009; Jones 2009; Tromeur and Rossow 2010). The WH04 RMM index is a combined cloudiness- and circulation-based index that has been frequently used by the community as a means for real-time prediction and definition of the MJO. The RMM index is created from a pair of empirical orthogonal functions (EOFs) of daily OLR, 200- and 850-hPa zonal wind fields. On a phase-space diagram, the principal components of the first two EOFs (RMM1 and RMM2, respectively) serve as the abscissa (RMM1) and ordinate (RMM2) axes (Fig. 1). One of the benefits of the RMM phase-space diagram is that it clearly indicates both geographical location (phase) and amplitude of the MJO, depending on the quadrant and radial distance from the center of each point on the diagram. Specifically, RMM amplitude is given by $(\text{RMM1}^2 + \text{RMM2}^2)^{1/2}$. Time progression through the phase-space diagram is typically in a counterclockwise fashion, representing the eastward propagation of the MJO.

The intensity of MJO activity has been quantified in many studies. One of the most commonly adopted intensity definitions is that of WH04, who defined active MJO to be one where RMM amplitude was greater than one. Consequently, most of the studies that use the RMM to quantify the MJO have only considered MJO

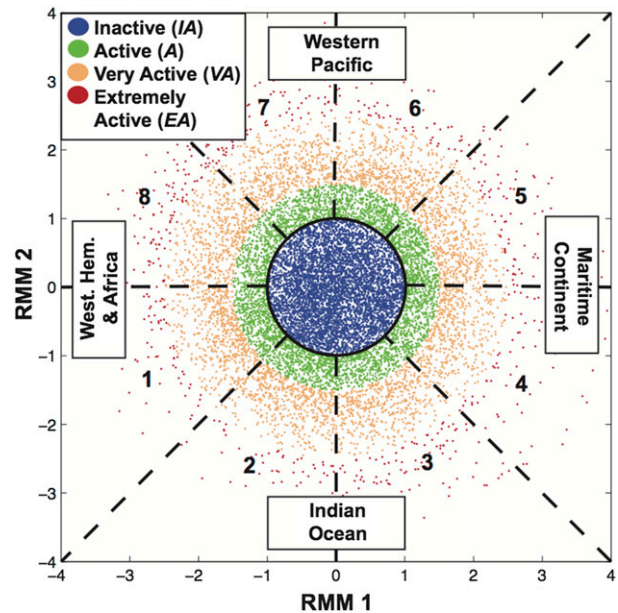


FIG. 1. Phase-space diagram of the RMM index (WH04) showing daily phase (quadrant) and magnitude (distance from center) of the MJO from 1 Jun 1974 through 31 Mar 2014. Colors indicate thresholds of activity: IA (blue, $\text{RMM} < 1.0$), A (green, $\text{RMM} \geq 1.0$ and < 1.5), VA (brown, $\text{RMM} \geq 1.5$ and < 2.5), and EA (red, $\text{RMM} \geq 2.5$).

events with an RMM amplitude greater than one. However, what is perhaps less known is that WH04 also defined a “more active” MJO, one where the square of the RMM amplitude was greater than 2.0. WH04 found this more active MJO to be most common in December–February (DJF) and March–May (MAM), and from the Centre for Australian Weather and Climate Research (CAWCR) operational RMM website (<http://cawcr.gov.au/staff/mwheeler/maproom/RMM/>), it is clear that MJO anomalies are strongest during DJF and MAM, weakest in June–August (JJA), and increasing in amplitude during September–November (SON). Similar to WH04, Yoo et al. (2012) defined active MJO as those occurrences having an RMM amplitude greater than 1.5, and they found that approximately 30% of November–March days from 1979 to 2008 met this criterion. This occurrence of MJO with amplitude greater than 1.5 was consistent with Garfinkel et al. (2012), who found 37% of November–March days to have an RMM amplitude greater than 1.5 from 1979 to 2011. In this study, we adopted the active threshold of WH04 and the very active thresholds of Yoo et al. (2012) and Garfinkel et al. (2012) and created two new thresholds, for a total of four categories of MJO activity. The remainder of this article is organized as follows: section 2 contains the data and methodology, results are presented in section 3, and discussion and conclusions are presented in section 4.

2. Data and methods

a. Data

All MJO calculations were based on the daily RMM MJO index, the version with the interannual signal removed (WH04). This seasonally independent index is based on a pair of EOFs of daily averaged OLR, 200- and 850-hPa zonal winds from the National Centers for Environmental Prediction (NCEP). The OLR is available in real time; however, zonal winds lag by a few days and operational analyses are used until they can be replaced with a reanalyzed version. Projection of daily observed data onto the multiple-variable EOFs yields two principal components (RMM1 and RMM2) that vary mostly on the intraseasonal time scale of the MJO. These principal components can be plotted on a phase-space diagram (Fig. 1), where each point denotes the phase (quadrant) and amplitude (distance from the center) of the MJO for a given day. RMM amplitude is the square root of the sum of the squares of RMM1 and RMM2, as defined earlier. The black circle in Fig. 1 represents an RMM amplitude of 1.0, which is the threshold for active MJO as defined by WH04. Each of the four colors in Fig. 1 denotes a different RMM activity threshold (activity thresholds are defined below in section 2b). The eastward propagation of the MJO is captured by a general counterclockwise motion between points (not shown here; see Fig. 7 in WH04), starting with phase 1 in the upper portion of the third quadrant of the diagram and ending with phase 8 in the lower portion of the second quadrant of the diagram. The phases represent the approximate geographical centers of the convection-favoring portion of the MJO, and corresponding geographical labels are provided on the edges of the diagram, following the designation of WH04.

The results in this study were based on over 40 years of daily RMM values, from 1 June 1974 through 31 March 2014, with approximately 2% of the time series missing from 17 March 1978 through 31 December 1978. The RMM index's success is based on its simplicity and real-time practicality; however, it is important to note that the RMM index is not without limitations. For example, the use of a single pair of EOFs helps provide simplicity, but it cannot capture subtle differences of every MJO event, which evolve with varying structures (Ventrice et al. 2013), and higher-frequency noise may also be present in the index due to the lack of a bandpass time filter (Roundy et al. 2009). Furthermore, the RMM index relies on large-scale circulation patterns for MJO detection and may not detect MJO initiation when these signals are absent (Straub 2013). Last, meridional averaging of OLR signals may pose difficulty in detecting MJO shifts across hemispheres (Ventrice et al. 2011).

Even with these limitations, the WH04 index has been used in many studies as the metric by which to quantify the MJO, and thus we have selected it as the basis for our climatology.

b. Methods

Several climatological aspects of the MJO were explored in this study. First, annual and seasonal variability of MJO intensity were quantified using four defined activity categories: inactive (IA), active (A), very active (VA), and extremely active (EA). Second, consecutive and subsequent occurrences in MJO activity were measured for the four above-defined categories. Third, duration and low-frequency (decadal) variability of complete MJO cycles was quantified. Finally, physical significance of MJO amplitude was explored for the different categories. WH04 defined A MJO days as those with amplitude greater than or equal to 1.0 and IA as MJO days as those with amplitude less than 1.0, and these two categorical definitions were adopted for this study. We added two new categories, VA and EA, to better understand the variability of MJO activity at the upper-end amplitudes. An MJO event was classified as VA if its amplitude reached or exceeded 1.5, and it was classified as EA if its amplitude reached or exceeded 2.5. We set these amplitude thresholds of VA and EA with the intent for them to include approximately 30% and 5% of MJO days, respectively. Both annual and seasonal relative frequencies were calculated for each of these four activity categories for each of the eight RMM phases. Annual relative frequency of MJO RMM amplitude was used to provide a baseline to examine seasonal variability (Fig. 2). The seasonal frequency distribution level (DJF, MAM, JJA, and SON) of both relative frequency and by phase and activity were then calculated (Fig. 3) and compared to the annual frequency (Fig. 2). Statistical significance of frequency anomalies was calculated using the Student's *t* test, and for this study, results significant at the 95% and 99% confidence levels were reported where found.

To investigate the persistence of MJO activity levels, the days immediately after each category of activity were examined using the following methodology. First, the number of occurrences of consecutive day events of a given activity level were counted. To accomplish this, each day was categorized by its activity level, and then the following days were examined to see if they had the same activity level. Once a day with a different activity level was found, the length of the event (e.g., the number of consecutive days with the same level of activity) was noted, and then counting began again, starting with that day. This climatology did not consider the MJO phase, only amplitude.

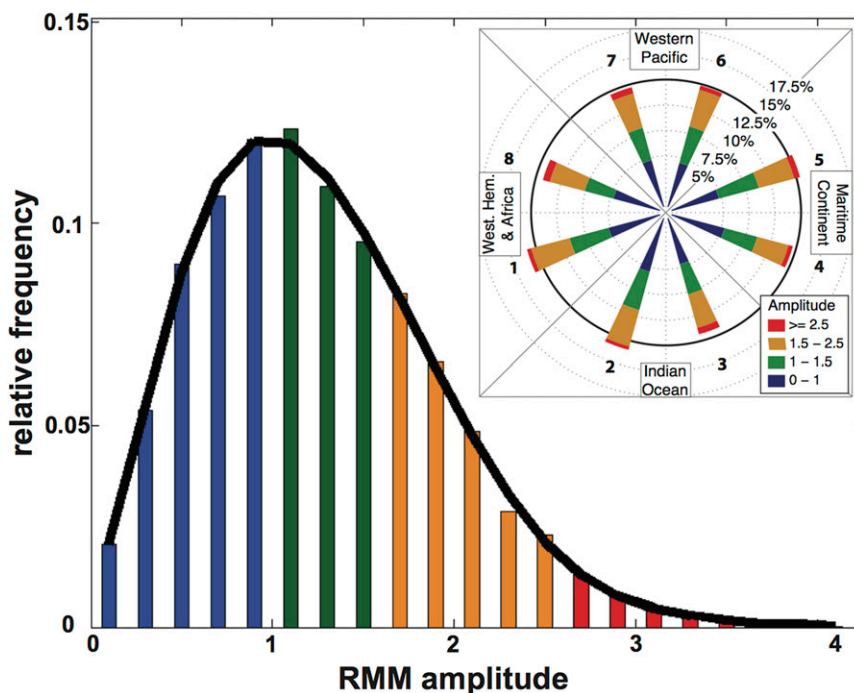


FIG. 2. Relative frequency of MJO RMM amplitude for all seasons (histogram) in addition to frequencies by phase and activity level (wind-rose-type diagram, top right). Dark curve on the histogram is a polynomial best fit to the histogram data with colors indicating MJO activity level. Colored segments on the wind rose denote the percent of mean annual occurrences in the given regions as the general geographical locations of MJO are given for pairs of phases. The colors represent the activity level of the given phase based on IA (blue), A (green), VA (brown), and EA (red) events.

To further examine daily MJO transitions, probabilities of subsequent-day activity levels were calculated based on the amplitude of the start date. Tallies of each category were then used to determine probabilities of each activity threshold being maintained on subsequent days. Similar to the consecutive-day climatology, this subsequent-day climatology only considered MJO amplitude, not RMM phase. To explore the length of a complete MJO cycle—that is, one in which the circulation and convective anomalies complete a circuit and end in the same geographical phase where they began—two approaches were used. First, the number and length of MJO events were counted that started active and stayed active as they circumnavigated the planet. The length of the event was established as the number of days it took the RMM index to return to the phase in which it began, again with the stipulation that the amplitude must remain active for the entire event. Following Jones (2009), the definition of active MJO was slightly relaxed to RMM amplitude >0.9 (instead of >1.0). This modification allowed for the counting of circumnavigating MJO events whose amplitudes weakened slightly below 1.0 but otherwise stayed above 0.9.

Second, the number and length of MJO events were counted that started and finished active, with the MJO still progressing eastward in the RMM phase, but they were allowed to weaken to any amplitude between its start and finish dates. Similar to the first count, the lengths of these events were established as the number of days it took the RMM index to return to the phase in which it began.

Finally, to explore the physical significance of MJO intensity, upper-tropospheric streamfunction ψ , taken from the NCEP–NCAR reanalyses (Kalnay et al. 1996), was correlated with RMM amplitude. Correlations were calculated for four categories of MJO amplitude: all amplitudes, all amplitudes greater than 1.0, all amplitudes greater than 1.5, and all amplitudes greater than 2.0. Correlations statistically significant at the 95% confidence level were found using a Student's t test. Streamfunction values at sigma level $\sigma = 0.2101$ were chosen because, for a pressure top of 50 hPa and a pressure bottom of 1000 hPa, sigma level 0.2101 corresponded to approximately 250 hPa. At that pressure level, the atmospheric response to MJO heating occurs via Rossby waves (Hendon and Salby 1994; Kiladis et al. 2005; Barlow 2012; Monteiro et al. 2014), which can then

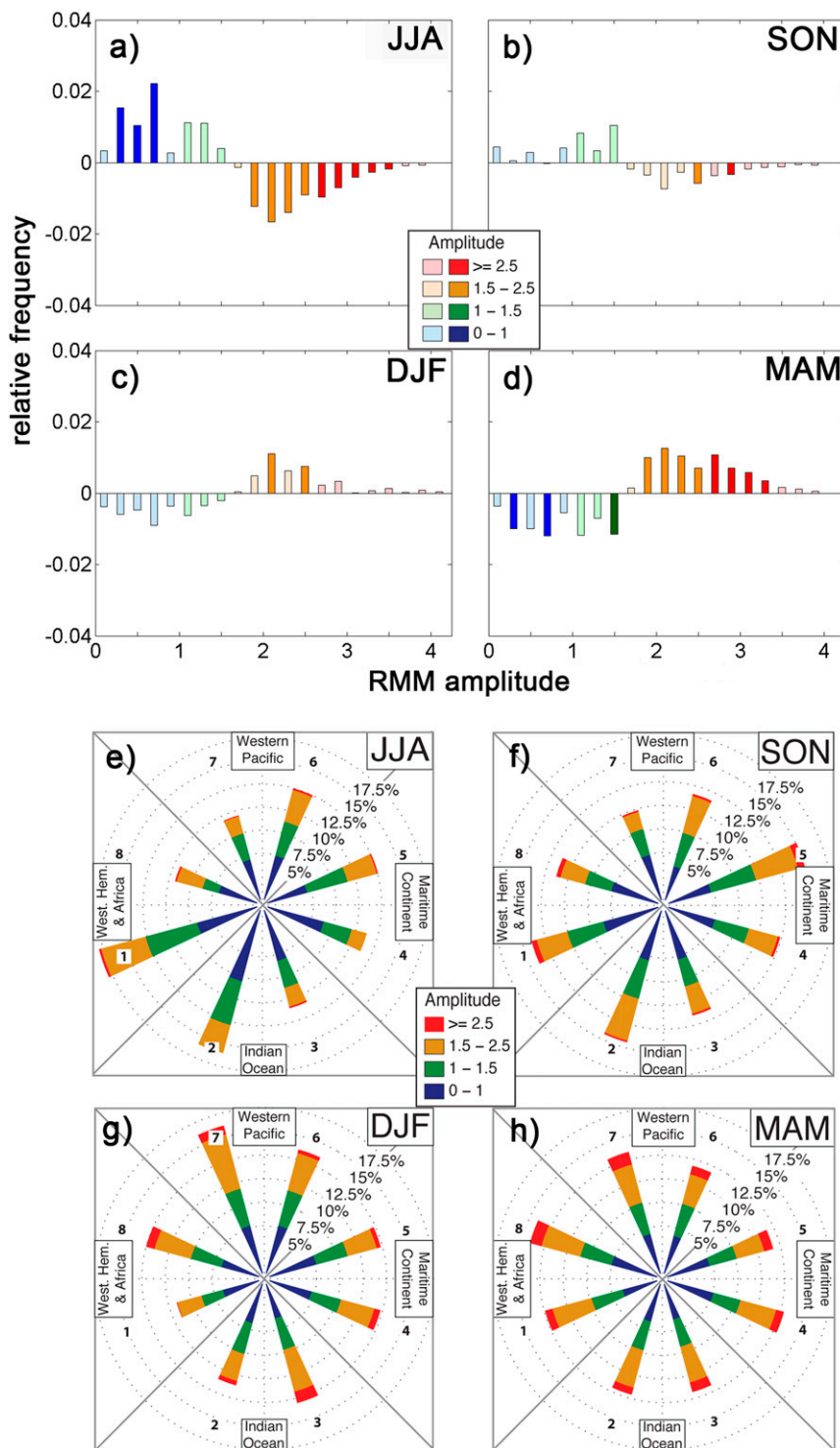


FIG. 3. Similar to Fig. 2, but for anomalous seasonal relative frequency of RMM amplitude for (a) JJA, (b) SON, (c) DJF, and (d) MAM in addition to frequencies by phase and activity level (e) JJA, (f) SON, (g) DJF, and (h) MAM, for 1 Jun 1974–31 Mar 2014. Colors indicate MJO activity level with dark colors in (a)–(d) indicating anomalies statistically significant at the 95% confidence level.

TABLE 1. Annual and seasonal percent occurrences by activity levels. Percent values shown in boldface (boldface and italics) indicate positive (negative) seasonal differences from the annual rate of occurrence that were statistically significant at the 99% confidence level.

Season	Level of activity	Percentage of season
Annual	Inactive	39.3
	Active	60.7
	Very active	32.6
	Extreme	4.2
JJA	Inactive	45.1
	Active	54.9
	Very active	24.8
	Extreme	1.0
SON	Inactive	40.5
	Active	59.5
	Very active	30.3
	Extreme	2.8
DJF	Inactive	36.5
	Active	63.5
	Very active	36.3
	Extreme	5.1
MAM	Inactive	35.0
	Active	65.0
	Very active	39.1
	Extreme	8.0

interact with the mean flow (Adames and Wallace 2014). Rossby waves exist in the lower troposphere as well; however, the structure and amplitude of the Rossby wave response in the upper-troposphere was the focus of this study.

3. Results

a. Phase and activity distribution: Annual

The first climatological aspect of the MJO that was developed was its annual and seasonal activity. Using the definitions of the activity levels given above, 39.3% of the days in this study were classified as IA and 60.7% were classified as A. Additionally, 32.6% of days were classified as VA and 4.2% were classified as EA (Table 1). Seasonal occurrences of MJO at the four activity levels were often different from annual occurrences (Table 1); positive differences that were statistically significant at the 99% confidence level are indicated as boldface text in Table 1, and negative differences are indicated with italics. The relative frequency of RMM amplitude in conjunction with distributions of annual phase and activity levels was also analyzed (Fig. 2; amplitudes colored). Across the entire year, MJO frequency peaked at an amplitude of approximately 1.0. However, it is unclear from the histogram alone if this distribution is representative of each phase. Thus, “wind rose” type depictions (Fig. 2, top right) featuring a layout

TABLE 2. Seasonal and annual phase occurrences expressed as percentages. Values are equivalent to the respective segment lengths in Figs. 2, 3 phase diagrams. Percent values shown in boldface (boldface and italics) indicate positive (negative) seasonal differences from the annual rate of occurrence that were statistically significant at the 99% confidence level.

	MJO phase							
	1	2	3	4	5	6	7	8
JJA	17.9	16.0	11.0	11.3	12.5	12.5	9.4	9.3
SON	14.0	14.4	11.5	12.3	15.1	11.6	9.8	11.3
DJF	9.1	11.1	13.0	12.3	12.3	13.6	16.2	12.5
MAM	12.4	12.1	11.8	12.9	11.7	11.8	13.3	14.1
Annual	13.4	13.4	11.8	12.2	12.9	12.4	12.2	11.8

similar to that of the WH04 RMM phase-space diagram were used to explore the frequency of each individual phase. The length of each segment shows the frequency at which that activity level occurs. Lengths for each phase were based on the mean annual percent occurrence of each phase (Table 2). Numbers in boldface indicate positive differences, and numbers in boldface and italics indicate negative differences; both boldface and boldfaced italics indicate statistical significance at the 99% confidence level. This even frequency distribution of 12.5% divided evenly among the eight RMM phases is denoted by the solid black circle in Fig. 2. Overall, the annual phase activity and phase occurrence distributions were relatively equal (Fig. 2; Table 2). The four colored sub-segments that compose each segment correspond to the percent occurrences of each of the four activity levels. For example, from June 1974 to March 2014, an MJO with an IA amplitude and in phase 1 occurred about 5% of the time, an MJO with an A amplitude and in phase 1 occurred about 8.5% of the time, an MJO with a VA amplitude and in phase 1 occurred about 4.5% of the time, and an MJO with an EA amplitude and in phase 1 occurred about 1% of the time. It is important to note that the A and VA segments correspond to a range of amplitudes that match their respective thresholds. For example, the green sub-segments only include RMM amplitudes greater than or equal to 1.0 and less than 1.5, but the frequency of days in the A category would include the sum of the green, brown, and red sub-segments because A is defined as having an RMM amplitude greater than or equal to 1.0. Annually, IA MJO days occurred approximately the same amount of time in all phases, as denoted by the length of the IA (blue) sub-segments of the segments. Similar occurrences were found for A, VA, and EA days, although phase 8 occurred least often but had the most frequent occurrence of EA days.

b. Phase and activity distribution: Seasonal

A second climatological aspect of the MJO developed for this study was its activity over the course of individual

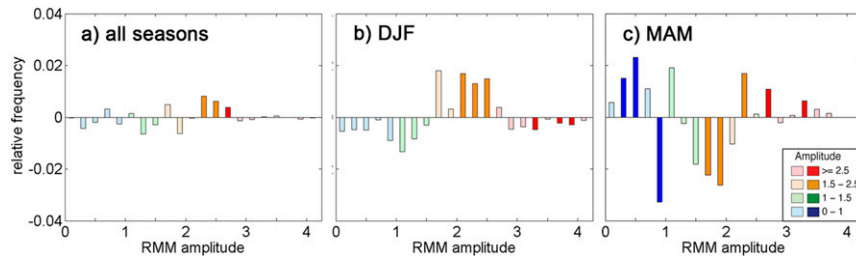


FIG. 4. Difference in relative frequency between two 20-yr periods: 1994–2013 minus 1974–93, for (a) all months, (b) only DJF, and (c) only MAM. Colors indicate MJO activity level, with dark colors indicating differences that are statistically significant at the 95% confidence level.

seasons. To do this, the relative frequency of RMM amplitude for each season was compared to the relative frequency of RMM amplitude for the entire year (Fig. 3). Anomalies in RMM amplitude showed where each season departed from the annual mean (Figs. 3a–d). The most significant differences were seen between MAM and JJA. In MAM (Fig. 3d), the frequency of IA amplitudes was statistically significantly below the annual mean and the frequency of VA and EA amplitudes was statistically significantly above the annual mean (darker colored bars in Fig. 3 indicate anomalies statistically significant at the 95% level). In contrast, in JJA (Fig. 3a), IA amplitudes occurred more often, and VA and EA amplitudes occurred less often. A similar, but less pronounced, contrast was seen between SON (Fig. 3b) and DJF (Fig. 3c): in SON, the frequency of VA and EA amplitudes was below normal, and in DJF, the frequency of VA amplitudes was above normal. These results agreed well with Madden (1986), Knutson and Weickmann (1987), Matthews et al. (1996), and Zhang and Dong (2004), who also found that active days were more common in DJF (Fig. 3g) and MAM (Fig. 3h) than in JJA (Fig. 3e) and SON (Fig. 3f) (63.5% and 65.0% for DJF and MAM versus 54.9% and 59.5% for JJA and SON). The most frequent occurrence of EA days (Fig. 3h, red sub-segments) was found in MAM, with EA days accounting for 8% of the season, while in JJA, EA days occurred only 1% of the time. These intraseasonal differences were also statistically significant at the 99% confidence level. It is interesting to note that, while JJA was overall the least active season for MJO, phase 8 showed unusually high levels of A and VA activity (compared to the other phases), perhaps as a result of the seasonal northward migration and convective strengthening of the intertropical convergence zone into the equatorial Western Hemisphere during JJA (e.g., Waliser and Gautier 1993; Grimm and Silva Dias 1995; Rydbeck et al. 2013; Neena et al. 2014; Roundy 2014). The distribution of EA frequency by the RMM phase

displayed a slightly different seasonal trend, with the least phase-to-phase variability in JJA and the most in DJF. This result highlights the phases where extreme MJO activity is more likely (e.g., during phase 3 in DJF and phase 7 in MAM) or less likely (e.g., during phase 1 in DJF and phase 2 in MAM).

The number of days in each phase also varied seasonally, with JJA and DJF displaying the most variability and SON and MAM the least variability (Fig. 3; Table 2). In JJA, phase 1 was the most frequent phase (17.9% of JJA days) and phase 8 was the least frequent (9.3% of JJA days) (Table 2). In SON, phase 5 occurred most often (15.1% of SON days) and phase 7 was the least frequent (9.8% of SON days). Phase 7 was the most frequent phase in DJF (16.2% of DJF days) and phase 1 was the least frequent (9.1% of DJF days). In MAM, phase 8 was the most frequent phase (14.1% of MAM days) and phase 5 was the least frequent phase (11.7% of MAM days). This trend can also be summarized by percent difference between most and least occurring phases (Table 2). In JJA, the difference was 8.5% compared to 7.1% in DJF. The difference decreased in SON to 5.2%, and the phase occurrence variability in MAM was similar to the mean annual distribution, with only a 1.6% difference between the most- and least-frequent phases. It is important to note that some of the phase-to-phase variability of the IA intensity category could be affected by noise, as the geographic location indicated by phase of an MJO event with very small RMM amplitude has little real physical significance.

Statistically significant differences in MJO amplitude, at the 95% confidence level, were also found between the first 20-yr period (1974–93) and the last 20-yr period (1994–2013) of the study (Fig. 4). For the year (Fig. 4a), the later period experienced more occurrences of high-intensity MJO events ($RMM > 2.0$) than the former period. These increases were primarily seen in DJF and MAM (Figs. 4b,c), with corresponding

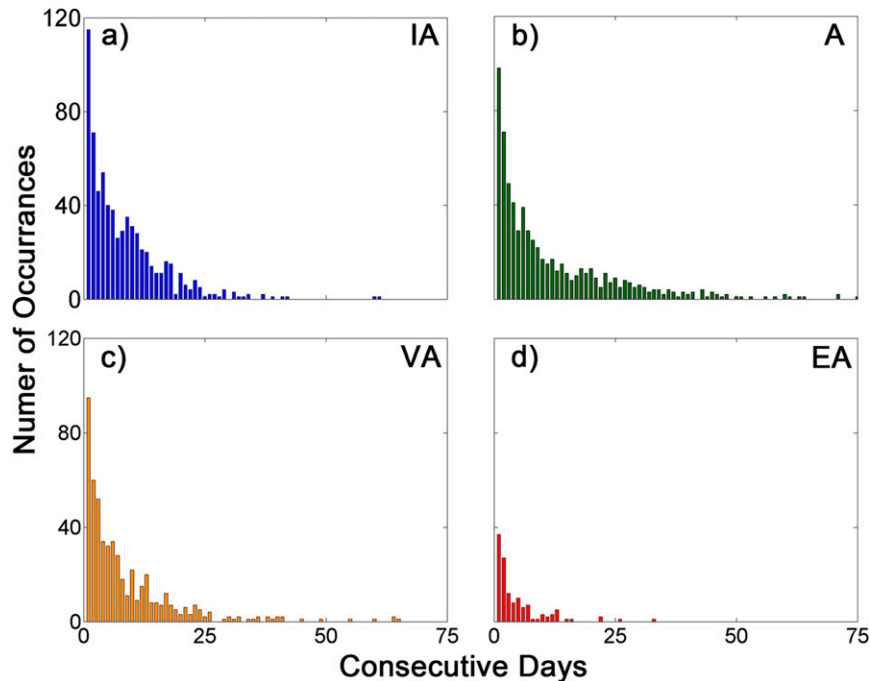


FIG. 5. Number of consecutive-day occurrences for each activity level (a) IA, (b) A, (c) VA, and (d) EA, for 1 Jun 1974–31 Mar 2014.

decreases in amplitudes between 1.0 and 2.0. This low-frequency variability both corroborates and extends the work of Jones and Carvalho (2006), who found the highest-amplitude Fourier harmonics during a 18.5-yr period and noted an increase in DJF MJO amplitude in the last 20 years compared to the first 20 yr. This study extends their work by finding similar low-frequency variability in MAM. Low-frequency variability in JJA and SON (not shown) was minimal and not statistically significant.

c. Consecutive occurrences

A third climatological aspect of the MJO that was developed was its daily persistence in the four activity levels. To calculate persistence, the number of consecutive daily MJO events in a particular phase was counted across the time series to estimate the probabilities of occurrence (Fig. 5). Shorter consecutive periods for all activity levels were most common, with an exponential decrease toward longer events. Short consecutive IA events, however, occurred more frequently than A events. For example, there were 116 instances when the MJO was IA for only two consecutive days and 99 instances for when the MJO was A for two consecutive days (Fig. 5a versus Fig. 5b). In addition, there were fewer long stretches of consecutive inactive days (e.g., more than 30 consecutive days inactive) compared to the long stretches of consecutive active days, suggesting that periods of consecutive

active MJO days longer than about a month were more common than consecutive inactive days (Figs. 5a,b). For example, only five periods occurred where MJO was persistently IA for over 40 days, while three A periods lasted over 90 days, and one of those lasted 154 days. Consecutive VA and EA day occurrences were also examined (Figs. 5c,d); however it should be noted that all VA and EA consecutive days represent subsets of A consecutive days (Fig. 5b). Periods of VA MJO rarely lasted over 30 consecutive days (24 instances); however, there were five instances of VA periods persisting for longer than 60 days (Fig. 5c). Consecutive EA periods lasting more than 10–15 days were relatively rare, with only four periods of consecutive EA longer than 20 days (Fig. 5d). The longest period of continuous IA days was 62, of continuous A days was 154, of continuous VA days was 85, and of continuous EA days was 33. Fitting a decay function of the form $f(x) = ae^{\alpha x}$ to each category yielded decay coefficients α of -0.15 (IA), -0.16 (A), -0.19 (VA), and -0.39 (EA) and goodness-of-fit coefficients (R^2) of 0.94, 0.94, 0.96, and 0.96, respectively. These decay coefficients confirmed that both IA, A, and VA MJO categories had similar patterns of consecutive-day occurrences, diminishing to near-zero occurrences beyond about day 45 (for IA and VA) and beyond about day 60 (for A). The decay coefficients also confirmed that there were fewer occurrences of

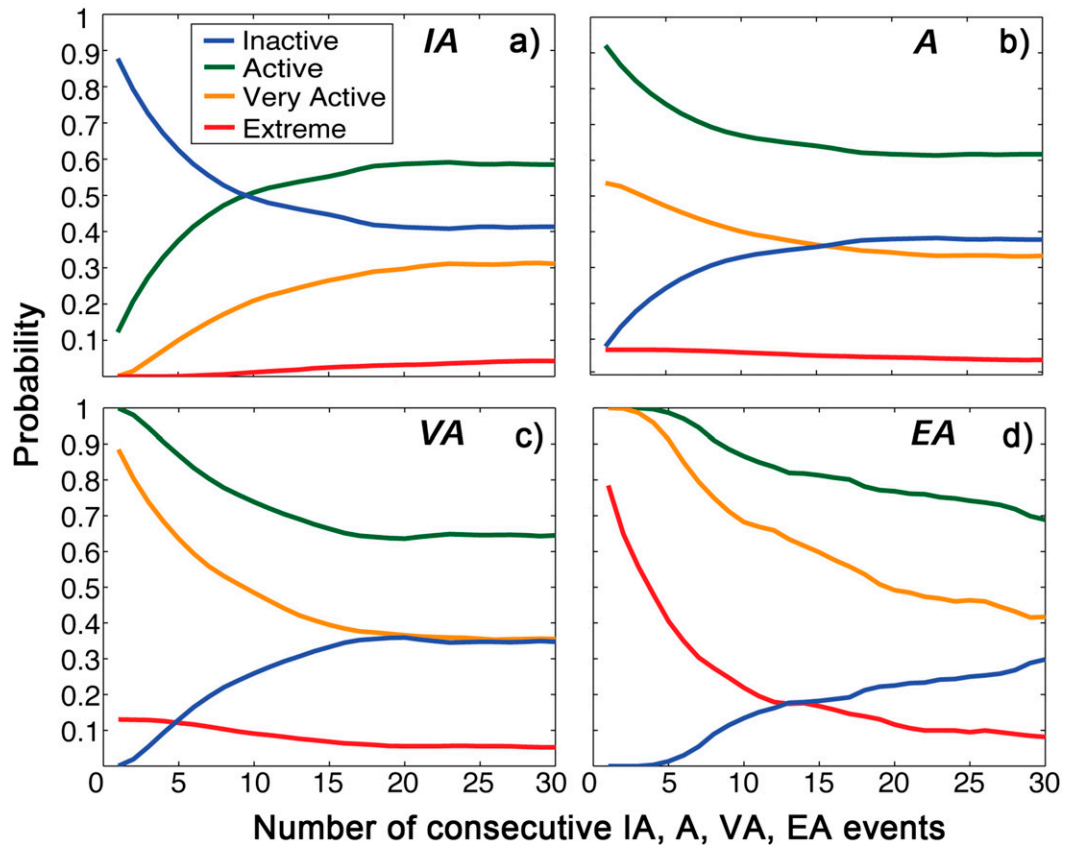


FIG. 6. Probability of subsequent categorical activity level. The four panels represent the activity level on the tested day. The four probability curves in each panel denote the likelihood that the days following would be a certain activity level, given that the starting day (day 0) was (a) IA, (b) A, (c) VA, or (d) EA.

consecutive EA categories, diminishing to near-zero occurrences beyond day 33.

d. Subsequent occurrences

A fourth climatological aspect of the MJO that was developed in this study was the probabilities of a subsequent categorical activity level (IA, A, VA, and EA) for days following each activity level (Fig. 6). For a given IA day (Fig. 6a), there was an 87.7% chance that the following day would be at the same level (IA), a 12.2% chance that the following day would be A, and a 0% chance that the following day would be VA or EA. With each subsequent day, the chance that the subsequent day would be IA decreased and the chance that the subsequent day would be A, VA, or EA increased. At approximately 10 days out from an IA day, the chances of that day being IA or A were even (both at 50%). For a given A day (Fig. 6b), the chance that a subsequent day would be A was high (greater than 70%) out to approximately day 7. For a given VA day (Fig. 6c), the chance that a subsequent day would be VA was high (greater than 50%) out to approximately day 9, and the chance that a

subsequent day would be A was very high (above 70%) out to approximately day 13. For a given EA day (Fig. 6d), the chance that a subsequent day would be EA was above 50% out to day 4, and the chance that a subsequent day would be at least A was nearly 100% out to day 5. These results confirm an important aspect of the MJO, namely, that its intensity is autocorrelated. However, they also suggest time scales for decorrelation of the MJO. For example, active, very active, and extremely active days were very likely (greater than 70% chance) to be followed by A, VA, and EA days. Even inactive MJO days were more likely to have transitioned to active MJO by day 10. Finally, by day 30, the probabilities of seeing each of the four MJO activity categories (IA, A, VA, and EA) trended toward the climatological occurrence values seen in Table 1 and Fig. 1 (40% chance of IA, 60% chance of A, 30% chance of VA, and 5% chance of EA).

e. MJO duration

As noted by Straub (2013) and Kiladis et al. (2014), one of the current challenges faced by researchers and forecasters studying the MJO is to define it. The MJO

itself is characterized by strong circulation anomalies, but the circulation anomalies themselves are at times either not associated with a convective signal (e.g., Weickmann and Berry 2009) or appear on satellite as an envelope of higher-frequency convective activity (Dias et al. 2013). One possible way to mitigate this challenge is to define a MJO event as one in which the circulation and convective anomalies complete a circuit, that is, where they circumnavigate the equator and end up in the general location where they began. In this climatology, we present two approaches to counting these “complete cycle” MJO events. First, we count the number and length of MJO events that start active and stay active as they circumnavigate the planet. The length of an event of this type would be the number of days the RMM index takes to return to the phase in which it began, with the stipulation that the RMM index must remain active during the entire cycle. For this section, the definition of an “active” MJO was slightly modified, following Jones (2009), in which an active MJO was defined as RMM amplitude >0.9 (instead of >1.0). This modification allowed for the counting of circumnavigating MJO events whose amplitudes weakened below 1.0 but stayed above 0.9. Second, we count the number and length of MJO events that start active and finish active, with the MJO still circumnavigating the planet but allowed to weaken below the active threshold. Similar to the first count, the length of an event of this second type would still be the number of days the RMM index takes to return to the phase in which it began, without the stipulation that it remain active for the entire cycle.

From 1974 to 2013, the shortest complete MJO cycle (one starting and ending in the same RMM phase) with MJO required to remain active for all days was 17 days (Fig. 7a). The longest MJO cycle was 61 days, and the mean cycle period was 34.1 days, out of a total of 78 events. (When the amplitude threshold of active MJO was set to 1.0, fewer events, 59 compared to 78, were identified than when the threshold was set to 0.9.) This mean period was shorter than the period reported by Madden and Julian (1972), who defined the oscillation as a 30–60-day cycle. This difference can be attributed to the requirement here for the oscillation to remain continuously active. When the “continuously active” requirement was relaxed (i.e., MJO events only needed to start and end as active), the shortest complete cycle was 14 days, the longest complete cycle was 151 days, and the mean cycle period was 54.1 days, out of a total of 260 events (Fig. 7b). This mean cycle period was toward the upper limit of the duration defined in Madden and Julian (1972) for return periods of pressure variability in the tropical western Pacific Ocean. Cycle durations were

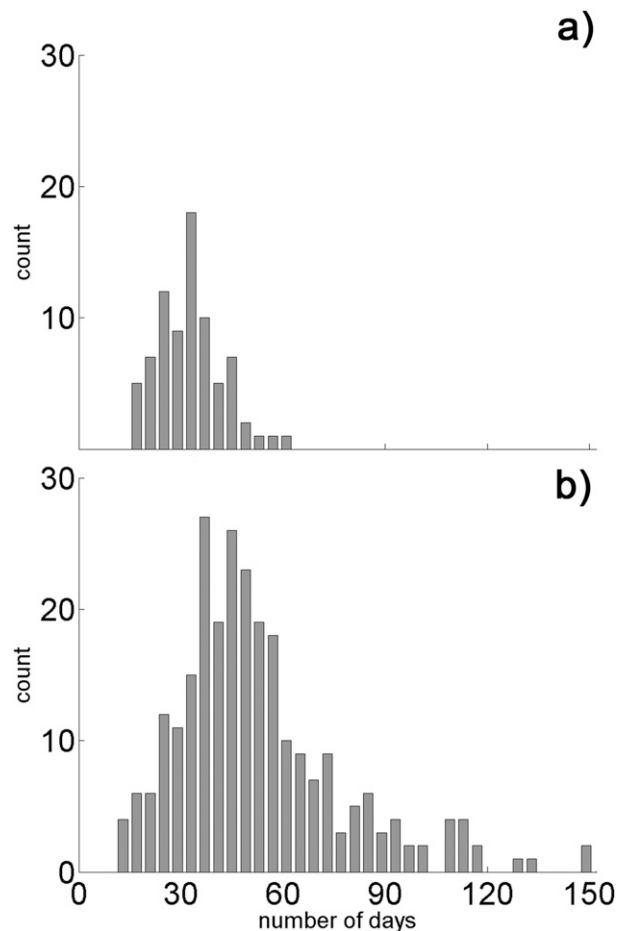


FIG. 7. Counts (in number of occurrences) of time to complete an MJO cycle. (a) All days must stay active, and (b), only the start and finishing days must be active.

not tested for phase or season. Thus, it is possible that cycle length variability is sensitive to either starting phase or season.

f. Physical significance of larger MJO amplitude

To conclude this climatological study, we present a brief physical application of the significance of MJO amplitude. To show the significance of MJO amplitude, linear correlations between upper-troposphere streamfunction ψ and MJO amplitude were calculated for MAM at $\sigma = 0.2101$ (approximately 250 hPa) for each grid in the NCEP–NCAR reanalyses (Kalnay et al. 1996). Phases 2 and 6 were selected for analysis because they occupy opposite corners of the RMM phase diagram; results were similar for other opposing phase pairs. March–May was selected because those months contained the most frequent occurrences of MJO amplitude above 2.0. For both phases, as MJO amplitude increased, the magnitude of correlations between MJO amplitude and ψ also increased (Fig. 8; only

correlations significant at the 95% confidence level are shown). Positive correlations were located along the equator, while negative correlations were located over the middle and high latitudes. This correlation pattern confirmed a linear upper-tropospheric response to MJO heating: equatorial streamfunction increased with increasing MJO amplitude, while extratropical streamfunction decreased with increasing MJO amplitude. Because nondivergent zonal wind speed is directly proportional to magnitude of the meridional gradient of ψ , $|u| = |-\partial\psi/\partial y|$, an increase in ψ at the equator combined with a decrease in ψ in the extratropics would yield greater zonal winds. The smallest correlations (magnitudes generally smaller than 0.4) were found between ψ and all MJO amplitudes (Figs. 8a,b), but correlations increased as the subset of MJO amplitudes (Figs. 8c,f) became more restrictive. The largest magnitude correlations were found between ψ and MJO amplitude for an MJO amplitude greater than 2.0 (Figs. 8g,h). This suggests that the greatest extratropical response in zonal wind speed amplification occurred for the strongest MJO events, in agreement with Hoell et al. (2014). Furthermore, the rate of change of the correlations increased with increasing MJO amplitude, seen as a larger increase in correlation in Figs. 8e–g than in Figs. 8a–d. The wavy pattern of extratropical streamfunction amplification in response to increased MJO amplitude (wavy pattern seen best in Figs. 8g,h extending from the North Pacific to the North Atlantic) agrees well with Hoskins and Karoly (1981), Ferranti et al. (1990), Hendon and Salby (1994), Matthews et al. (2004), Kiladis et al. (2005), Barlow (2012), Bao and Hartmann (2014), and Adames and Wallace (2014), who all found a similar planetary-scale wavy-pattern response in the extratropics to tropical heating anomalies. While not a new result, this finding does confirm that the extremity of MJO amplitude is important to consider when exploring tropical–extratropical teleconnections.

4. Discussion and conclusions

Previous climatological studies of the MJO have found that the amplitude of the MJO varies more during boreal winter and spring months than during boreal summer and autumn months (WH04; Zhang and Dong 2004). The MJO has also been shown to have RMM amplitudes greater than 1.5 between 30% (Yoo et al. 2012) and 37% (Garfinkel et al. 2012) of the days since 1974. The results presented in this paper agreed well with these earlier papers and extended them in five key ways. First, when the entire year is considered, the frequency of days in each MJO phase was nearly identical

at about 12.5% for each phase, with phase 8 less likely (11.8%) than phases 1 or 2 (13.4%). Furthermore, the frequency of the four categorical definitions of MJO activity (inactive, active, very active, and extremely active, defined as RMM amplitudes less than 1.0 and greater than or equal to 1.0, 1.5, and 2.5, respectively) was also uniform throughout the year.

Second, when examined by season, clear patterns of variability were evident. For example, in JJA, a day when MJO convection was in phase 1 was nearly twice as likely as a day in phase 8, and that ratio generally extended to each of the four activity categories for those two phases. In DJF, phase 7 was the most common and phase 1 the least common, indicating a shift away from MJO activity in the Western Hemisphere and Africa when compared to JJA (Maloney and Hartmann 2000). This difference is likely driven by seasonality in tropical convection in both the western Pacific and the Western Hemisphere and Africa, whereby tropical convective activity is more favored in the equatorial Western Hemisphere during JJA than it is during DJF and more favored in the equatorial western Pacific during DJF than it is during JJA. Another major finding in seasonal variability of MJO intensity was seen in the frequency of EA days. For example, in MAM, the occurrence of EA days was notable, with all eight RMM phases reaching EA levels up to 8% of the time. This fraction of EA days was the largest of any season and contrasted sharply with JJA, when hardly any EA days were observed. The high relative frequency of EA days in MAM is likely driven by pronounced seasonality of the tropical atmosphere, as the convective anomalies associated with the MJO not only migrate northward into the Northern Hemisphere during MAM but also intensify, particularly over the eastern and central Pacific. This also suggests that the global, teleconnected response to tropical convective heating may be maximized in MAM, given that the most frequent occurrence of EA MJO is in that season. However, additional work is needed to further examine the consequences of EA MJO activity in each season.

Third, the number of consecutive days in each intensity category showed that the amplitude of the MJO was persistent in time, and persistent for all four intensity categories. This persistence was particularly seen at the A level, with the highest number of consecutive-day active MJO events (20-plus consecutive days) of the four categories.

Fourth, probability curves further confirmed the persistent nature of MJO events. For example, for all four of the activity categories, the following day had at least an 80% chance (and for categorical A MJO, a greater than 90% chance) of having the same activity category.

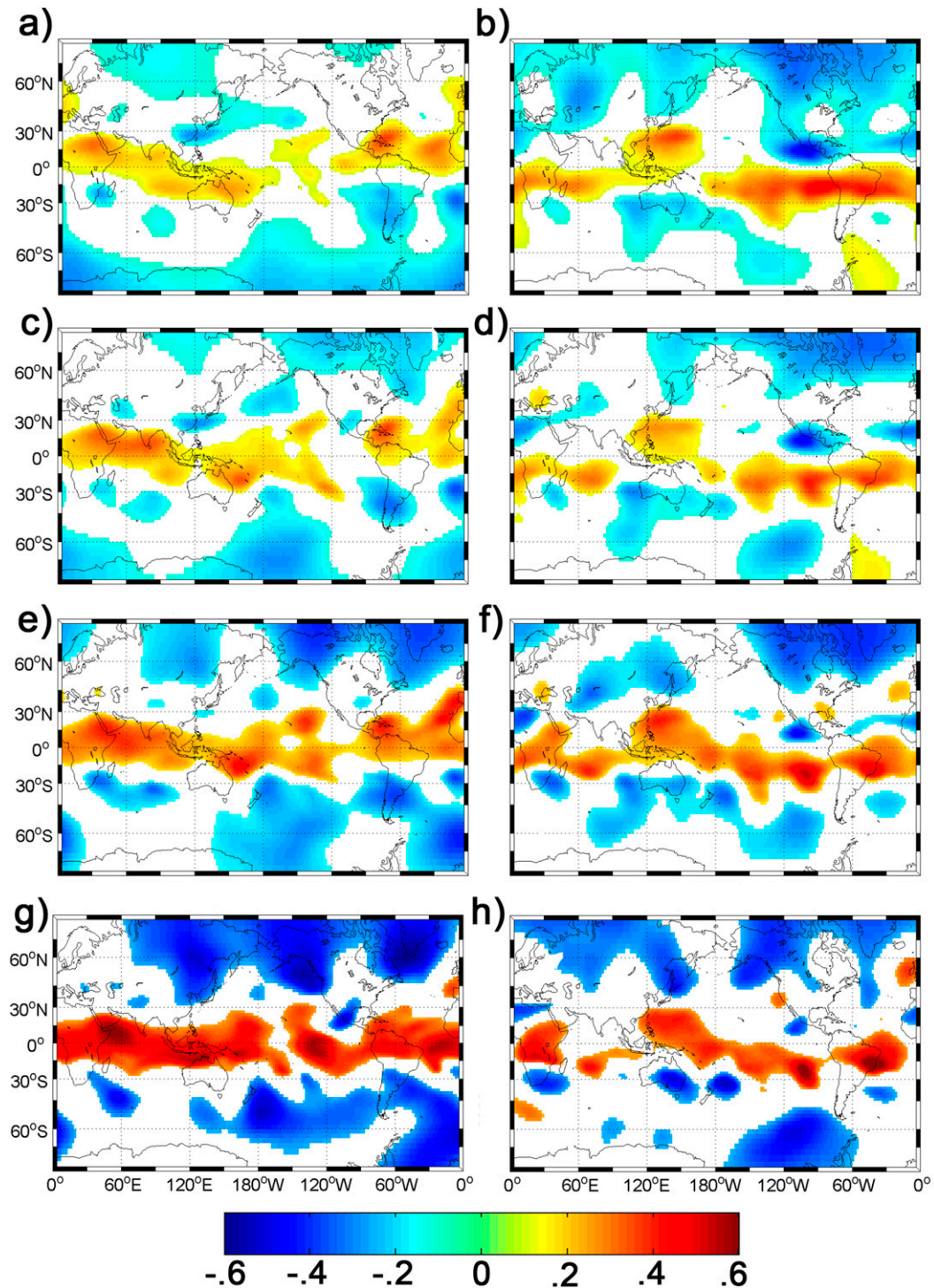


FIG. 8. Correlation coefficient (r) between MJO amplitude and 250-hPa streamfunction, for (a),(b) all MJO amplitudes; (c),(d) only A MJO amplitudes; (e),(f) only VA MJO amplitudes; and (g),(h) only MJO amplitudes >2.0 . Correlations for RMM (left) phase 2 and (right) phase 6. Other MJO phase pairings showed similar results.

For inactive MJO, the probability of returning to active was greater than 50% after day 10. Additionally, for very active and extremely active occurrences, the probability of becoming inactive in the subsequent 5 days was less than 10% (and nearly 0% for EA). As another example of persistence, even events characterized as extremely active MJO had nearly a 50% chance of still being extremely active 5 days later. At 30 days out, the probabilities for all four activity levels trended toward the climatology (60% chance of active, 40% chance inactive, 30% chance very active, and 5% chance extremely active).

Finally, the importance of quantifying extremity of MJO convection was shown in correlations between 250-hPa streamfunction and different subsets of MJO amplitudes. Magnitude of MJO convection was shown to amplify the waviness of 250-hPa streamfunction anomalies. Statistically significant correlations between MJO amplitude and streamfunction increased with MJO categories, and the largest-magnitude correlations were found for the strongest MJO amplitudes. Furthermore, because nondivergent zonal wind components are directly related to gradients in streamfunction, larger correlations confirm that the atmospheric response to the MJO depends on the magnitude of the convective heating anomaly.

These five climatological aspects of the MJO extend earlier studies that quantified both geographic location and intensity of MJO-related convection. One of the most important uses of this climatology is that it provides a framework and context to activity level, and here we defined two additional levels beyond those of **WH04**: very active, which occurred 32.6% of the time annually, and extremely active, which occurred about 4.2% of the time annually. Both of these categorical definitions exhibited statistically significant seasonality, particularly the extremely active category, which was rarely seen in JJA but present on 8% of the days in MAM. Furthermore, the relative frequency of consecutive-day MJO events was quantified for the first time, giving additional context to the rarity of MJO events that persist for several consecutive days at higher magnitudes. Finally, future work is needed to continue exploring the relationship between MJO amplitude and atmospheric response, specifically with a focus on possible seasonality or variability by starting phase.

Acknowledgments. This work was partially supported by NSF Grants PLR-1203843 and AGS-1240143. The authors thank the three anonymous reviewers for their helpful comments, which greatly strengthened this manuscript.

REFERENCES

- Adames, A. F., and J. M. Wallace, 2014: Three-dimensional structure and evolution of the MJO and its relation to the mean flow. *J. Atmos. Sci.*, **71**, 2007–2026, doi:[10.1175/JAS-D-13-0254.1](https://doi.org/10.1175/JAS-D-13-0254.1).
- Bao, M., and D. L. Hartmann, 2014: The response to MJO-like forcing in a nonlinear shallow-water model. *Geophys. Res. Lett.*, **41**, 1322–1328, doi:[10.1002/2013GL057683](https://doi.org/10.1002/2013GL057683).
- Barlow, M., 2012: Africa and West Asia. *Intraseasonal Variability in the Atmosphere-Ocean Climate System*, W. K.-M. Lau and D. E. Waliser, Eds., Springer Praxis Books, 477–495.
- Benedict, J. J., and D. A. Randall, 2007: Observed characteristics of the MJO relative to maximum rainfall. *J. Atmos. Sci.*, **64**, 2332–2354, doi:[10.1175/JAS3968.1](https://doi.org/10.1175/JAS3968.1).
- Chen, Y., and A. D. Del Genio, 2009: Evaluation of tropical cloud regimes in observations and a general circulation model. *Climate Dyn.*, **32**, 355–369, doi:[10.1007/s00382-008-0386-6](https://doi.org/10.1007/s00382-008-0386-6).
- Dias, J., S. Leroux, S. N. Tulich, and G. N. Kiladis, 2013: How systematic is organized tropical convection within the MJO? *Geophys. Res. Lett.*, **40**, 1420–1425, doi:[10.1002/grl.50308](https://doi.org/10.1002/grl.50308).
- Ferranti, L., T. N. Palmer, F. Molteni, and E. Klinker, 1990: Tropical-extratropical interaction associated with the 30–60 day oscillation and its impact on medium and extended range prediction. *J. Atmos. Sci.*, **47**, 2177–2199, doi:[10.1175/1520-0469\(1990\)047<2177:TEIAWT>2.0.CO;2](https://doi.org/10.1175/1520-0469(1990)047<2177:TEIAWT>2.0.CO;2).
- Garfinkel, C. I., S. B. Feldstein, D. W. Waugh, C. Yoo, and S. Lee, 2012: Observed connection between stratospheric sudden warmings and the Madden-Julian Oscillation. *Geophys. Res. Lett.*, **39**, L18807, doi:[10.1029/2012GL053144](https://doi.org/10.1029/2012GL053144).
- Grimm, A. M., and P. L. Silva Dias, 1995: Analysis of tropical-extratropical interactions with influence functions of a barotropic model. *J. Atmos. Sci.*, **52**, 3538–3555, doi:[10.1175/1520-0469\(1995\)052<3538:AOTIWI>2.0.CO;2](https://doi.org/10.1175/1520-0469(1995)052<3538:AOTIWI>2.0.CO;2).
- Hendon, H. H., and M. L. Salby, 1994: The life cycle of the Madden-Julian oscillation. *J. Atmos. Sci.*, **51**, 2225–2237, doi:[10.1175/1520-0469\(1994\)051<2225:TLCOTM>2.0.CO;2](https://doi.org/10.1175/1520-0469(1994)051<2225:TLCOTM>2.0.CO;2).
- , C. Zhang, and J. D. Glick, 1999: Interannual variation of the Madden-Julian oscillation during austral summer. *J. Climate*, **12**, 2538–2550, doi:[10.1175/1520-0442\(1999\)012<2538:IVOTMJ>2.0.CO;2](https://doi.org/10.1175/1520-0442(1999)012<2538:IVOTMJ>2.0.CO;2).
- Hoell, A., M. Barlow, M. C. Wheeler, and C. Funk, 2014: Disruptions of El Niño–Southern Oscillation teleconnections by the Madden-Julian oscillation. *Geophys. Res. Lett.*, **41**, 998–1004, doi:[10.1002/2013GL058648](https://doi.org/10.1002/2013GL058648).
- Hoskins, B. J., and D. J. Karoly, 1981: The steady linear response of a spherical atmosphere to thermal and orographic forcing. *J. Atmos. Sci.*, **38**, 1179–1196, doi:[10.1175/1520-0469\(1981\)038<1179:TSLROA>2.0.CO;2](https://doi.org/10.1175/1520-0469(1981)038<1179:TSLROA>2.0.CO;2).
- Jones, C., 2009: A homogeneous stochastic model of the Madden-Julian oscillation. *J. Climate*, **22**, 3270–3288, doi:[10.1175/2008JCLI2609.1](https://doi.org/10.1175/2008JCLI2609.1).
- , and L. M. V. Carvalho, 2006: Changes in the activity of the Madden-Julian oscillation during 1958–2004. *J. Climate*, **19**, 6353–6370, doi:[10.1175/JCLI3972.1](https://doi.org/10.1175/JCLI3972.1).
- Kalnay, E., and Coauthors, 1996: The NCEP/NCAR 40-Year Reanalysis Project. *Bull. Amer. Meteor. Soc.*, **77**, 437–471, doi:[10.1175/1520-0477\(1996\)077<0437:TNYRP>2.0.CO;2](https://doi.org/10.1175/1520-0477(1996)077<0437:TNYRP>2.0.CO;2).
- Kemball-Cook, S. R., and B. C. Weare, 2001: The onset of convection in the Madden-Julian oscillation. *J. Climate*, **14**, 780–793, doi:[10.1175/1520-0442\(2001\)014<0780:TOOCIT>2.0.CO;2](https://doi.org/10.1175/1520-0442(2001)014<0780:TOOCIT>2.0.CO;2).
- Kessler, W. S., 2001: EOF representations of the Madden-Julian oscillation and its connection with ENSO.

- J. Climate*, **14**, 3055–3061, doi:10.1175/1520-0442(2001)014<3055:EROTMJ>2.0.CO;2.
- Kiladis, G. N., and K. M. Weickmann, 1992: Circulation anomalies associated with tropical convection during northern winter. *Mon. Wea. Rev.*, **120**, 1900–1923, doi:10.1175/1520-0493(1992)120<1900:CAAWTC>2.0.CO;2.
- , K. H. Straub, and P. T. Haertel, 2005: Zonal and vertical structure of the Madden–Julian oscillation. *J. Atmos. Sci.*, **62**, 2790–2809, doi:10.1175/JAS3520.1.
- , M. C. Wheeler, P. T. Haertel, K. H. Straub, and P. E. Roundy, 2009: Convectively coupled equatorial waves. *Rev. Geophys.*, **47**, RG2003, doi:10.1029/2008RG000266.
- , J. Dias, K. H. Straub, M. C. Wheeler, S. N. Tulich, K. Kikuchi, K. M. Weickmann, and M. J. Ventrice, 2014: A comparison of OLR and circulation-based indices for tracking the MJO. *Mon. Wea. Rev.*, **142**, 1697–1715, doi:10.1175/MWR-D-13-00301.1.
- Knutson, T. R., and K. M. Weickmann, 1987: 30–60 day atmospheric oscillations: Composite life cycles of convection and circulation anomalies. *Mon. Wea. Rev.*, **115**, 1407–1436, doi:10.1175/1520-0493(1987)115<1407:DAOCLC>2.0.CO;2.
- Lawrence, D. M., and P. J. Webster, 2002: The boreal summer intraseasonal oscillation: Relationship between northward and eastward movement of convection. *J. Atmos. Sci.*, **59**, 1593–1606, doi:10.1175/1520-0469(2002)059<1593:TBSIOR>2.0.CO;2.
- Madden, R. A., 1986: Seasonal variations of the 40–50 day oscillation in the tropics. *J. Atmos. Sci.*, **43**, 3138–3158, doi:10.1175/1520-0469(1986)043<3138:SVOTDO>2.0.CO;2.
- , and P. R. Julian, 1971: Detection of a 40–50 day oscillation in the zonal wind in the tropical Pacific. *J. Atmos. Sci.*, **28**, 702–708, doi:10.1175/1520-0469(1971)028<0702:DOADOI>2.0.CO;2.
- , and —, 1972: Description of global-scale circulation cells in the tropics with a 40–50 day period. *J. Atmos. Sci.*, **29**, 1109–1123, doi:10.1175/1520-0469(1972)029<1109:DOGCC>2.0.CO;2.
- , and —, 1994: Observations of the 40–50-day tropical oscillation—A review. *Mon. Wea. Rev.*, **122**, 814–837, doi:10.1175/1520-0493(1994)122<0814:OOTDIO>2.0.CO;2.
- Majda, A. J., and S. N. Stechmann, 2012: Multiscale theories for the MJO. *Intraseasonal Variability in the Atmosphere–Ocean Climate System*, W. K. M. Lau and D. E. Waliser, Eds., Springer-Praxis, 1–20.
- Maloney, E. D., and D. L. Hartmann, 2000: Modulation of eastern North Pacific hurricanes by the Madden–Julian oscillation. *J. Climate*, **13**, 1451–1460, doi:10.1175/1520-0442(2000)013<1451:MOENPH>2.0.CO;2.
- Masunaga, H., 2007: Seasonality and regionality of the Madden–Julian oscillation, Kelvin wave, and equatorial Rossby wave. *J. Atmos. Sci.*, **64**, 4400–4416, doi:10.1175/2007JAS2179.1.
- Matthews, A. J., 2000: Propagation mechanisms for the Madden–Julian oscillation. *Quart. J. Roy. Meteor. Soc.*, **126**, 2637–2651, doi:10.1002/qj.49712656902.
- , 2008: Primary and successive events in the Madden–Julian oscillation. *Quart. J. Roy. Meteor. Soc.*, **134**, 439–453, doi:10.1002/qj.224.
- , and G. N. Kiladis, 1999: The tropical–extratropical interaction between high-frequency transients and the Madden–Julian oscillation. *Mon. Wea. Rev.*, **127**, 661–677, doi:10.1175/1520-0493(1999)127<0661:TTEIBH>2.0.CO;2.
- , B. J. Hoskins, J. M. Slingo, and M. Blackburn, 1996: Development of convection along the SPCZ within a Madden–Julian oscillation. *Quart. J. Roy. Meteor. Soc.*, **122**, 669–688, doi:10.1002/qj.49712253106.
- , —, and M. Masutani, 2004: The global response to tropical heating in the Madden–Julian oscillation during northern winter. *Quart. J. Roy. Meteor. Soc.*, **130**, 1991–2011, doi:10.1256/qj.02.123.
- Milliff, R. F., and R. A. Madden, 1996: The existence and vertical structure of fast, eastward-moving disturbances in the equatorial troposphere. *J. Atmos. Sci.*, **53**, 586–597, doi:10.1175/1520-0469(1996)053<0586:TEAVSO>2.0.CO;2.
- Monteiro, J. M., A. F. Adames, J. M. Wallace, and J. S. Sukhatme, 2014: Interpreting the upper level structure of the Madden–Julian oscillation. *Geophys. Res. Lett.*, **41**, 9158–9165, doi:10.1002/2014GL062518.
- Myers, D. S., and D. E. Waliser, 2003: Three-dimensional water vapor and cloud variations associated with the Madden–Julian oscillation during Northern Hemisphere winter. *J. Climate*, **16**, 929–950, doi:10.1175/1520-0442(2003)016<0929:TDWVAC>2.0.CO;2.
- Neena, J. M., X. Jiang, D. Waliser, J.-Y. Lee, and B. Wang, 2014: Eastern Pacific intraseasonal variability: A predictability perspective. *J. Climate*, **27**, 8869–8883, doi:10.1175/JCLI-D-14-00336.1.
- Pohl, B., and A. J. Matthews, 2007: Observed changes in the life-time and amplitude of the Madden–Julian oscillation with interannual ENSO sea surface temperature anomalies. *J. Climate*, **20**, 2659–2674, doi:10.1175/JCLI4230.1.
- Roundy, P. E., 2014: Some aspects of Western Hemisphere circulation and the Madden–Julian oscillation. *J. Atmos. Sci.*, **71**, 2027–2039, doi:10.1175/JAS-D-13-0210.1.
- , and W. M. Frank, 2004: A climatology of waves in the equatorial region. *J. Atmos. Sci.*, **61**, 2105–2132, doi:10.1175/1520-0469(2004)061<2105:ACOWIT>2.0.CO;2.
- , C. J. Schreck III, and M. A. Janiga, 2009: Contributions of convectively coupled equatorial Rossby waves and Kelvin waves to the real-time multivariate MJO indices. *Mon. Wea. Rev.*, **137**, 469–478, doi:10.1175/2008MWR2595.1.
- Rui, H., and B. Wang, 1990: Development characteristics and dynamic structure of tropical intraseasonal convection anomalies. *J. Atmos. Sci.*, **47**, 357–379, doi:10.1175/1520-0469(1990)047<0357:DCADSO>2.0.CO;2.
- Rydbeck, A. V., E. D. Maloney, S. P. Xie, J. Hafner, and J. Shaman, 2013: Remote forcing versus local feedback of east Pacific intraseasonal variability during boreal summer. *J. Climate*, **26**, 3575–3596, doi:10.1175/JCLI-D-12-00499.1.
- Salby, M. L., and H. H. Hendon, 1994: Intraseasonal behavior of clouds, temperature, and motion in the tropics. *J. Atmos. Sci.*, **51**, 2207–2224, doi:10.1175/1520-0469(1994)051<2207:IBOCTA>2.0.CO;2.
- Sardeshmukh, P. D., and B. J. Hoskins, 1988: The generation of global rotational flow by steady idealized tropical divergence. *J. Atmos. Sci.*, **45**, 1228–1251, doi:10.1175/1520-0469(1988)045<1228:TGGGRF>2.0.CO;2.
- Straub, K. H., 2013: MJO initiation in the real-time multivariate MJO index. *J. Climate*, **26**, 1130–1151, doi:10.1175/JCLI-D-12-00074.1.
- Tromeur, E., and W. B. Rossow, 2010: Interaction of deep tropical convection with the large-scale circulation in the MJO. *J. Climate*, **23**, 1837–1853, doi:10.1175/2009JCLI3240.1.
- Ventrice, M. J., C. D. Thorncroft, and P. E. Roundy, 2011: The Madden–Julian oscillation’s influence on African easterly waves and downstream tropical cyclogenesis. *Mon. Wea. Rev.*, **139**, 2704–2722, doi:10.1175/MWR-D-10-05028.1.
- , M. C. Wheeler, H. H. Hendon, C. J. Schreck III, C. D. Thorncroft, and G. N. Kiladis, 2013: A modified multivar-

- iate Madden–Julian oscillation index using velocity potential. *Mon. Wea. Rev.*, **141**, 4197–4210, doi:[10.1175/MWR-D-12-00327.1](https://doi.org/10.1175/MWR-D-12-00327.1).
- Waliser, D. E., and C. Gautier, 1993: A satellite-derived climatology of the ITCZ. *J. Climate*, **6**, 2162–2174, doi:[10.1175/1520-0442\(1993\)006<2162:ASDCOT>2.0.CO;2](https://doi.org/10.1175/1520-0442(1993)006<2162:ASDCOT>2.0.CO;2).
- Weickmann, K., and E. Berry, 2009: The tropical Madden–Julian oscillation and the global wind oscillation. *Mon. Wea. Rev.*, **137**, 1601–1614, doi:[10.1175/2008MWR2686.1](https://doi.org/10.1175/2008MWR2686.1).
- Wheeler, M. C., and G. N. Kiladis, 1999: Convectively coupled equatorial waves: Analysis of clouds and temperature in the wavenumber–frequency domain. *J. Atmos. Sci.*, **56**, 374–399, doi:[10.1175/1520-0469\(1999\)056<0374:CCEWAO>2.0.CO;2](https://doi.org/10.1175/1520-0469(1999)056<0374:CCEWAO>2.0.CO;2).
- , and H. H. Hendon, 2004: An all-season real-time multivariate MJO index: Development of an index for monitoring and prediction. *Mon. Wea. Rev.*, **132**, 1917–1932, doi:[10.1175/1520-0493\(2004\)132<1917:AARMMI>2.0.CO;2](https://doi.org/10.1175/1520-0493(2004)132<1917:AARMMI>2.0.CO;2).
- , G. N. Kiladis, and P. J. Webster, 2000: Large-scale dynamical fields associated with convectively coupled equatorial waves. *J. Atmos. Sci.*, **57**, 613–640, doi:[10.1175/1520-0469\(2000\)057<0613:LSDFAW>2.0.CO;2](https://doi.org/10.1175/1520-0469(2000)057<0613:LSDFAW>2.0.CO;2).
- Yoo, C., S. Lee, and S. B. Feldstein, 2012: Mechanisms of Arctic surface air temperature change in response to the Madden–Julian oscillation. *J. Climate*, **25**, 5777–5790, doi:[10.1175/JCLI-D-11-00566.1](https://doi.org/10.1175/JCLI-D-11-00566.1).
- Zhang, C., 2005: Madden-Julian Oscillation. *Rev. Geophys.*, **43**, RG2003, doi:[10.1029/2004RG000158](https://doi.org/10.1029/2004RG000158).
- , 2013: Madden–Julian oscillation: Bridging weather and climate. *Bull. Amer. Meteor. Soc.*, **94**, 1849–1870, doi:[10.1175/BAMS-D-12-00026.1](https://doi.org/10.1175/BAMS-D-12-00026.1).
- , and M. Dong, 2004: Seasonality in the Madden–Julian oscillation. *J. Climate*, **17**, 3169–3180, doi:[10.1175/1520-0442\(2004\)017<3169:SITMO>2.0.CO;2](https://doi.org/10.1175/1520-0442(2004)017<3169:SITMO>2.0.CO;2).